UCRL-JC-128019
PREPRINT

Classical Rayleigh-Taylor Instability Experiments at Nova

K. S. Budil
B. A. Remington
S. V. Weber
T. S. Perry
T. A. Peyser

This paper was prepared for submittal to the
39th Annual Meeting of the American Physical Society
Division of Plasma Physics
Pittsburgh, PA
November 17-21, 1997

November 10, 1997

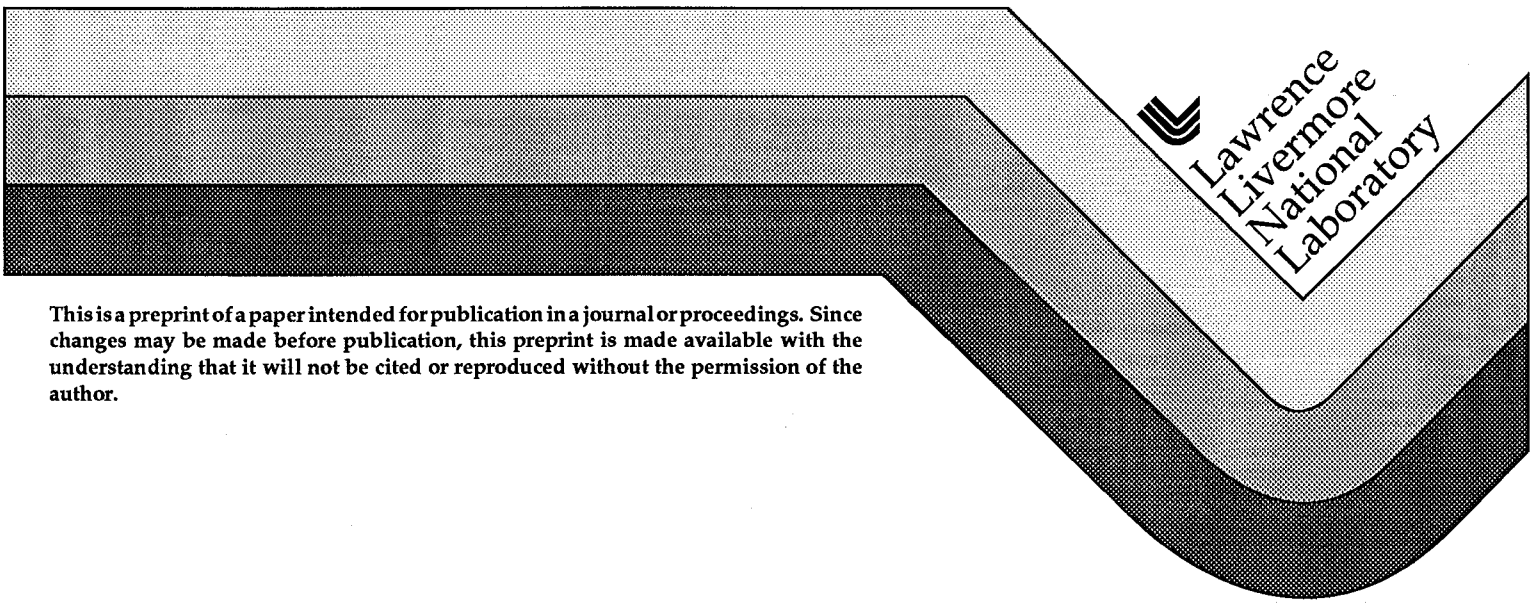

Classical Rayleigh-Taylor Instability Experiments at Nova

K. S. Budil, B. A. Remington, S. V. Weber, T. S. Perry and T. A. Peyser

Lawrence Livermore National Laboratory, P. O. Box 808, L-473

Livermore, CA 94551, email: budil1@llnl.gov

The evolution of the Rayleigh-Taylor (RT) instability at an embedded, or classical, interface is examined in a series of experiments at the Nova laser facility.{reference for Nova} These experiments focused on the transition from the linear to nonlinear regimes for both single- and multimode initial perturbations. The development of a single mode at the embedded interface is compared to its evolution at an ablation front and the effect of ablative stabilization is experimentally demonstrated. The multimode experiments have shown evidence of the process of *bubble competition*, wherein neighboring structures either continue to rise or are washed downstream in the flow depending upon their relative size. The experiments are compared with simulations performed with either the LASNEX code {G. B. Zimmerman and W. L. Kruer, Comments Plasma Phys. Controlled Fusion **2**, 51 (1975).}, a two-dimensional Lagrangian radiation-hydrodynamics code, or CALE {R. Tipton, reference for CALE}, a two-dimensional arbitrary Lagrange-Eulerian radiation-hydrodynamics code.

PACS numbers 52.35.Py, 47.40.Nm, 52.50.Lp, 52.70.La.

I. INTRODUCTION

Hydrodynamic instabilities are present in a wide variety of physical systems, from inertial confinement fusion (ICF) capsules to supernovae. In particular, the Rayleigh-Taylor (RT) instability,[1,2] wherein a heavy fluid is accelerated by a light fluid, is found in a variety of situations over an immense range of length and time scales. For ICF the imploding capsule goes through two phases of instability in both direct and indirect drive geometries. In the initial phases of the implosion the ablating outer surface of the capsule is RT unstable. As the implosion progresses and the outer layer of the capsule, the "pusher", begins to decelerate, the inner fuel-pusher interface becomes unstable.[3-6] At the opposite end of the spectrum of length and time scales lie astrophysical examples of hydrodynamic instabilities. Astrophysicists seeking to explain the early appearance of spectral signatures from heavy elements produced at the core of an exploding star believe that large growth of RT bubbles and spikes at density "interfaces" allows the heavier elements to penetrate through the outer layers of the star much earlier than would be expected just from one-dimensional expansion plus diffusion.[7,8]

We have performed a series of experiments to investigate the evolution of single- and multimode perturbations at an RT-unstable, embedded interface. The growth of single mode perturbations at an embedded interface is markedly different from that at an ablation front. At an

ablation front, short wavelengths are strongly stabilized while at the embedded interface these wavelengths exhibit the highest growth factors observed. This was a conclusive experimental demonstration of ablative stabilization and is described elsewhere.[9] Here we describe the evolution of single mode perturbations with wavelengths of λ = 10, 20 and 50 μm and initial amplitudes of η_o = 0.5 and 1.0 μm utilizing a longer x ray drive which yields a longer period of acceleration for the experimental foils.

The behavior of a multimode spectrum is very different from that of a single mode. At an ablation front, the growth of a collection of initial modes can be described by a model proposed by Haan.[10] The growth can be divided into two stages: (1) a linear regime where growth is exponential and (2) a nonlinear regime approximated by an asymptotic, constant bubble velocity. Because ablation will stabilize the shortest wavelengths and the longer-wavelength modes may not have particularly large amplitudes, this model, which neglects mode coupling, reasonably describes the evolution of a wide, smooth initial spectrum.

However, in the case of an embedded interface, isolated from the influence of ablation, short wavelength modes (λ ~ 10-20 μm) grow strongly.[9] For this case, where growth of longer wavelengths can be due primarily to seeding via mode coupling rather from their initial amplitudes, the development of the mixing region should lose dependence upon the initial conditions.[11,12] The bubble front penetration is given by $\eta_o = \alpha A g t^2$ and the front evolution can be described in statistical terms from the dynamics of the

individual bubbles plus two-bubble merger.[11-14] As the coupling proceeds, longer and longer wavelength structures will begin to dominate the flow resulting in an *inverse cascade.* Here we have performed experiments with initial perturbations consisting of a superposition of 2, 10 and 20 initial modes.

This paper is organized as follows. In Sec. II we describe the experimental configuration and target fabrication. Sec. III and Sec. IV describe the results of the single mode and two-mode experiments respectively. The multimode (20 modes) experiments are discussed in Sec. V and Sec. VI contains a summary and the conclusions we have drawn from this work.

II. EXPERIMENTAL CONFIGURATION

The experimental configuration is illustrated in Figure 1. In the experiments described herein, eight of the ten beams of the Nova laser at a wavelength of .351 μm are focused into a 3-mm-long by 1.6-mm-diameter gold cylindrical hohlraum to generate a 4.3 ns low-adiabat, shaped drive. This was used to ablatively-accelerate a 750 μm diameter planar foil mounted over a hole in the hohlraum. The laser temporal profile and the corresponding radiation temperature history are shown in Figure 2(a).

The target foil was diagnosed using face-on radiography. An iron foil was irradiated by the remaining two Nova beams at a wavelength .528 or .351 μm and with a 2 or 3 ns pulse duration to generate Fe He-α x rays at 6.7 keV to back-illuminate the target. Random phase plates (.528 μm light)[15] or

kinoform phase plates (.351 μm light)[16] were inserted into the backlighter beamlines to generate a smooth ~750 μm diameter spot. Two-dimensional radiographs of each target were recorded with a temporally gated x-ray framing camera.[17] The radiographs were then Fourier-analyzed to determine perturbation amplitude in ℓn(exposure) $\propto$ -δ(OD) as a function of time, where OD represents optical depth.

The sample foils consisted of a 40 μm thick CH(Br) ($C_{50}H_{47}Br_3$, ρ = 1.26 g/cm^3) ablator backed by a 15 μm thick Ti (ρ = 4.5 g/cm^3) payload. The perturbation being studied was placed at the CH(Br)-Ti interface and consisted of either two, ten or twenty cosine modes superimposed in phase. The hohlraum radiation drive has been characterized and was confirmed here with trajectory measurements with the composite foils with no perturbations at the CH(Br)-Ti interface. These measurements were then compared to calculations using the LASNEX code[18] and are shown in Figure 2(b). The very large spike at 1.5 ns is due to the passage of the first shock through the experimental package, prior to the compressed foil beginning to accelerate as a whole. In contrast to the prior experiments investigating the behavior of single mode perturbations at the embedded interface[9] which utilized a 3.3 ns low adiabat drive, the laser power profile utilized here provides a longer period of reasonably constant acceleration.

Both the single- and multimode targets investigated had a perturbation precision machined at the CH(Br)-Ti interface.[19] The targets were made by machining the required perturbation onto a copper mandrel and then

sputter-coating this with Ti. The Cu mandrel was then acid etched away and the CH(Br) layer was hot pressed onto the rippled Ti surface. The perturbations were characterized by atomic force microscopy and contact radiography and are known to better that 10%.

III. SINGLE MODE EXPERIMENTS

As described previously[9], a series of experiments was performed to investigate the behavior of single mode perturbations at an embedded interface. Four wavelengths were studied, λ = 10 μm (η_o = 0.5 μm), 20 μm (η_o = 1.0 μm), 50 μm (η_o = 1.0 μm), and 100 μm (η_o = 1.0 μm). An x-ray drive with a shorter duration (3.3 ns) was utilized for these experiments and is described in detail elsewhere.[9,20,21] An example of the radiographic data obtained for the 20 μm wavelength at t = 4.6 ns is shown in Figure 3(a). Figure 3(b) contains the growth factor (GF = $\eta(t)/\eta_o$) observed for this perturbation as a function of time (solid circles) compared to a LASNEX simulation (solid curve). The simulation is in reasonable agreement with the data, particularly at early times, although it underpredicts the highest growth factor observed.

In order to best demonstrate the differences between perturbation evolution at the embedded interface to that at an ablation front, a normalized growth factor was constructed. The GF for each wavelength at t = 3.2 ns, a time before the onset of significant nonlinearity, was normalized to the GF for λ = 50 μm at this time in both the data and the LASNEX simulations. The

same quantity was constructed for a series of GF simulations and measurements made for perturbations placed at the ablation front of a solid CH(Br) target which was accelerated in a similar fashion to the two-layer target.[9,20,21] These normalized GF are displayed in Figure 4. This comparison between ablation front and embedded interface growth dramatically illustrates the influence of ablative stabilization. While ablation strongly stabilizes short wavelengths, these wavelengths exhibit the highest growth factors observed at the embedded interface. This distinction makes the CH(Br)-Ti embedded interface target an ideal testbed for studying instability evolution in the nonlinear regime, particularly the processes of nonlinear mode coupling and bubble competition.

IV. TWO MODE EXPERIMENTS

A. Mode coupling in Fourier space

After completion of the single-mode experiments described, we began to examine the behavior of an initial spectrum of two or more modes. A modal model for the evolution of such a perturbation where mode coupling is the dominant source of long wavelength structures in the flow is described by Ofer *et al.* [13] Initially, two readily-resolvable initial modes (λ = 10 μm, η_o = 1 μm and λ = 15 μm, η_o = 1 μm) were superimposed in phase. As the growth of the two initial modes proceeds into the nonlinear regime they begin to couple, producing "beat" modes $k_i \pm k_j$, the amplitude of which can be written at second order as

$$\eta_{k_i \pm k_j} \sim (1/2)(k_i \pm k_j)\, \eta_{k_i}^{L}\, \eta_{k_j}^{L} \qquad (1)$$

where $\eta_{k_i}^{L}$ is the spatial amplitude of the mode k_i had the growth been entirely in the linear regime.[11] Here the $k_{\lambda = 10\,\mu m} - k_{\lambda = 15\,\mu m} = k_{\lambda = 30\,\mu m}$ (λ = 30 μm) beat mode should be observed growing up in time.

Figure 5 contains a series of averaged lineouts from the data (left axis) as well as the original pattern (right axis, solid line) imposed at the embedded interface. The curves correspond to lineouts at t = 3.8 ns (dotted curve), 4.3 ns (dashed curve), 4.9 ns (long dashed curve), and 5.3 ns (dot-dashed curve). The imposed pattern is seen growing as time progresses, but the two latest times show a striking qualitative difference from the early time lineouts. The short scale (10 and 15 μm) structures are beginning to give way to a longer scale (30 μm) envelope. By 5.3 ns this effect is quite marked and Fourier analysis should show the amplitude of this longer wavelength mode increasing in time.

A comparison of the Fourier amplitudes of the three modes observed in ℓn(exposure) and the CALE simulations convolved with the instrument MTF is shown in Figure 6. The data and simulations show reasonable agreement and, indeed, a mode at λ = 30 μm, generated from the mode coupling between the 10 and 15 μm modes in the initial spectrum, is observed growing up strongly in the data.

This experiment is an illustration of the process which drives a multimode spectrum toward an inverse cascade late in the nonlinear

development of the instability. A long wavelength feature has been generated via mode coupling between the initial modes, not from the growth of an initially imposed mode. This Fourier-space observation is compelling evidence of the importance of mode coupling processes at a classical, or embedded, interface where stabilization mechanisms for short wavelengths are not present. This process has also been described in terms of a bubble competition process, wherein large structures will, over time, begin to wash smaller-scale structures in the flow downstream. This dominance of large structures will appear as a preponderance of low mode numbers in the Fourier spectrum, which after several generations of mode coupling results in an inverse cascade.

B. Bubble competition in physical space

In the work of Alon *et al.*,[22] the competition between neighboring bubbles is described in a physically-intuitive manner. They begin with an initial velocity field composed of a sum of two modes with wave numbers k and 2k and amplitudes u_1 and u_2, which corresponds to two bubbles with velocities $u_1 \pm u_2$. At early times, the bubbles are seen to rise independently. However, as time progresses the large bubble begins to expand and rise faster, washing its smaller neighbor downstream in the flow. We designed our second two mode experiment to directly investigate the evolution of neighboring bubbles of different sizes as described by Alon. Our target consisted of a superposition of two modes with wave numbers k and 2k

UCRL-JC-128019
PREPRINT

Classical Rayleigh-Taylor Instability Experiments at Nova

K. S. Budil
B. A. Remington
S. V. Weber
T. S. Perry
T. A. Peyser

This paper was prepared for submittal to the
39th Annual Meeting of the American Physical Society
Division of Plasma Physics
Pittsburgh, PA
November 17-21, 1997

November 10, 1997

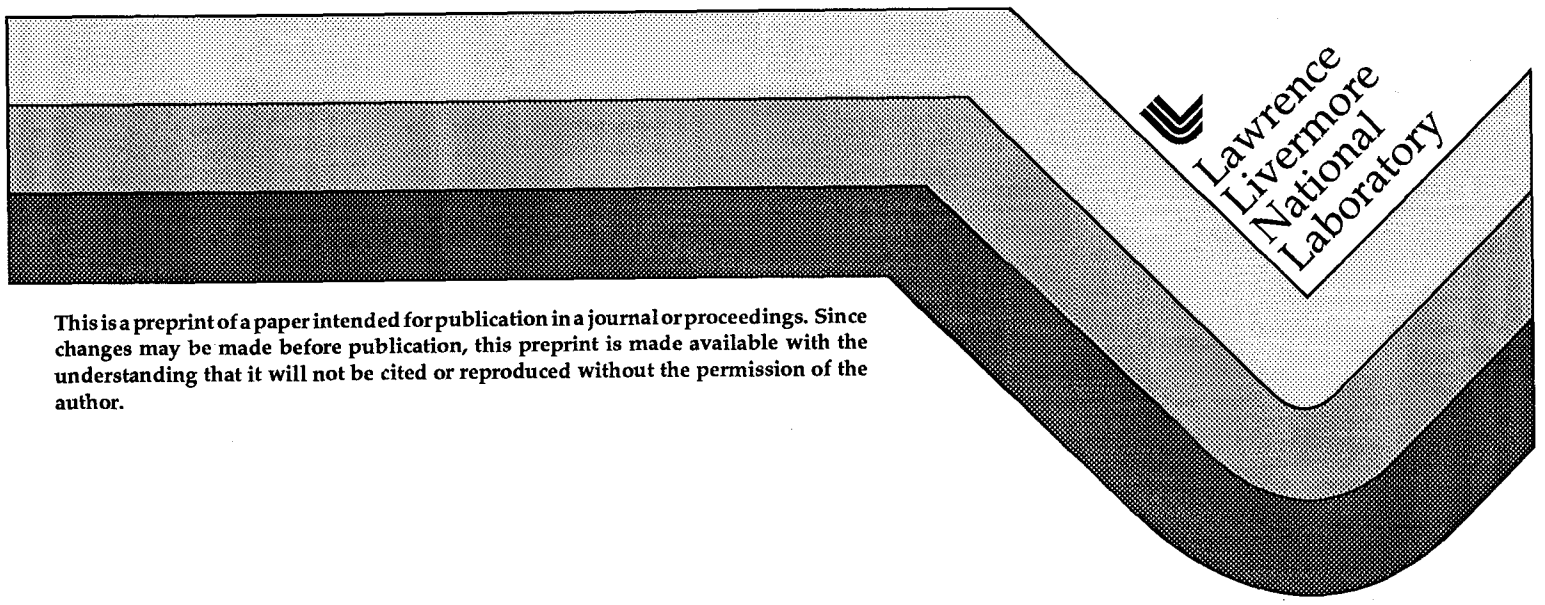

Classical Rayleigh-Taylor Instability Experiments at Nova

K. S. Budil, B. A. Remington, S. V. Weber, T. S. Perry and T. A. Peyser

Lawrence Livermore National Laboratory, P. O. Box 808, L-473

Livermore, CA 94551, email: budil1@llnl.gov

The evolution of the Rayleigh-Taylor (RT) instability at an embedded, or classical, interface is examined in a series of experiments at the Nova laser facility.{reference for Nova} These experiments focused on the transition from the linear to nonlinear regimes for both single- and multimode initial perturbations. The development of a single mode at the embedded interface is compared to its evolution at an ablation front and the effect of ablative stabilization is experimentally demonstrated. The multimode experiments have shown evidence of the process of *bubble competition*, wherein neighboring structures either continue to rise or are washed downstream in the flow depending upon their relative size. The experiments are compared with simulations performed with either the LASNEX code {G. B. Zimmerman and W. L. Kruer, Comments Plasma Phys. Controlled Fusion **2**, 51 (1975).}, a two-dimensional Lagrangian radiation-hydrodynamics code, or CALE {R. Tipton, reference for CALE}, a two-dimensional arbitrary Lagrange-Eulerian radiation-hydrodynamics code.

PACS numbers 52.35.Py, 47.40.Nm, 52.50.Lp, 52.70.La.

I. INTRODUCTION

Hydrodynamic instabilities are present in a wide variety of physical systems, from inertial confinement fusion (ICF) capsules to supernovae. In particular, the Rayleigh-Taylor (RT) instability,[1,2] wherein a heavy fluid is accelerated by a light fluid, is found in a variety of situations over an immense range of length and time scales. For ICF the imploding capsule goes through two phases of instability in both direct and indirect drive geometries. In the initial phases of the implosion the ablating outer surface of the capsule is RT unstable. As the implosion progresses and the outer layer of the capsule, the "pusher", begins to decelerate, the inner fuel-pusher interface becomes unstable.[3-6] At the opposite end of the spectrum of length and time scales lie astrophysical examples of hydrodynamic instabilities. Astrophysicists seeking to explain the early appearance of spectral signatures from heavy elements produced at the core of an exploding star believe that large growth of RT bubbles and spikes at density "interfaces" allows the heavier elements to penetrate through the outer layers of the star much earlier than would be expected just from one-dimensional expansion plus diffusion.[7,8]

We have performed a series of experiments to investigate the evolution of single- and multimode perturbations at an RT-unstable, embedded interface. The growth of single mode perturbations at an embedded interface is markedly different from that at an ablation front. At an

ablation front, short wavelengths are strongly stabilized while at the embedded interface these wavelengths exhibit the highest growth factors observed. This was a conclusive experimental demonstration of ablative stabilization and is described elsewhere.[9] Here we describe the evolution of single mode perturbations with wavelengths of λ = 10, 20 and 50 μm and initial amplitudes of η_o = 0.5 and 1.0 μm utilizing a longer x ray drive which yields a longer period of acceleration for the experimental foils.

The behavior of a multimode spectrum is very different from that of a single mode. At an ablation front, the growth of a collection of initial modes can be described by a model proposed by Haan.[10] The growth can be divided into two stages: (1) a linear regime where growth is exponential and (2) a nonlinear regime approximated by an asymptotic, constant bubble velocity. Because ablation will stabilize the shortest wavelengths and the longer-wavelength modes may not have particularly large amplitudes, this model, which neglects mode coupling, reasonably describes the evolution of a wide, smooth initial spectrum.

However, in the case of an embedded interface, isolated from the influence of ablation, short wavelength modes (λ ~ 10-20 μm) grow strongly.[9] For this case, where growth of longer wavelengths can be due primarily to seeding via mode coupling rather from their initial amplitudes, the development of the mixing region should lose dependence upon the initial conditions.[11,12] The bubble front penetration is given by $\eta_o = \alpha A g t^2$ and the front evolution can be described in statistical terms from the dynamics of the

individual bubbles plus two-bubble merger.[11-14] As the coupling proceeds, longer and longer wavelength structures will begin to dominate the flow resulting in an *inverse cascade.* Here we have performed experiments with initial perturbations consisting of a superposition of 2, 10 and 20 initial modes.

This paper is organized as follows. In Sec. II we describe the experimental configuration and target fabrication. Sec. III and Sec. IV describe the results of the single mode and two-mode experiments respectively. The multimode (20 modes) experiments are discussed in Sec. V and Sec. VI contains a summary and the conclusions we have drawn from this work.

II. EXPERIMENTAL CONFIGURATION

The experimental configuration is illustrated in Figure 1. In the experiments described herein, eight of the ten beams of the Nova laser at a wavelength of .351 μm are focused into a 3-mm-long by 1.6-mm-diameter gold cylindrical hohlraum to generate a 4.3 ns low-adiabat, shaped drive. This was used to ablatively-accelerate a 750 μm diameter planar foil mounted over a hole in the hohlraum. The laser temporal profile and the corresponding radiation temperature history are shown in Figure 2(a).

The target foil was diagnosed using face-on radiography. An iron foil was irradiated by the remaining two Nova beams at a wavelength .528 or .351 μm and with a 2 or 3 ns pulse duration to generate Fe He-α x rays at 6.7 keV to back-illuminate the target. Random phase plates (.528 μm light)[15] or

kinoform phase plates (.351 μm light)[16] were inserted into the backlighter beamlines to generate a smooth ~750 μm diameter spot. Two-dimensional radiographs of each target were recorded with a temporally gated x-ray framing camera.[17] The radiographs were then Fourier-analyzed to determine perturbation amplitude in ℓn(exposure) $\propto -\delta$(OD) as a function of time, where OD represents optical depth.

The sample foils consisted of a 40 μm thick CH(Br) ($C_{50}H_{47}Br_3$, ρ = 1.26 g/cm^3) ablator backed by a 15 μm thick Ti (ρ = 4.5 g/cm^3) payload. The perturbation being studied was placed at the CH(Br)-Ti interface and consisted of either two, ten or twenty cosine modes superimposed in phase. The hohlraum radiation drive has been characterized and was confirmed here with trajectory measurements with the composite foils with no perturbations at the CH(Br)-Ti interface. These measurements were then compared to calculations using the LASNEX code[18] and are shown in Figure 2(b). The very large spike at 1.5 ns is due to the passage of the first shock through the experimental package, prior to the compressed foil beginning to accelerate as a whole. In contrast to the prior experiments investigating the behavior of single mode perturbations at the embedded interface[9] which utilized a 3.3 ns low adiabat drive, the laser power profile utilized here provides a longer period of reasonably constant acceleration.

Both the single- and multimode targets investigated had a perturbation precision machined at the CH(Br)-Ti interface.[19] The targets were made by machining the required perturbation onto a copper mandrel and then

sputter-coating this with Ti. The Cu mandrel was then acid etched away and the CH(Br) layer was hot pressed onto the rippled Ti surface. The perturbations were characterized by atomic force microscopy and contact radiography and are known to better that 10%.

III. SINGLE MODE EXPERIMENTS

As described previously[9], a series of experiments was performed to investigate the behavior of single mode perturbations at an embedded interface. Four wavelengths were studied, λ = 10 μm (η_o = 0.5 μm), 20 μm (η_o = 1.0 μm), 50 μm (η_o = 1.0 μm), and 100 μm (η_o = 1.0 μm). An x-ray drive with a shorter duration (3.3 ns) was utilized for these experiments and is described in detail elsewhere.[9,20,21] An example of the radiographic data obtained for the 20 μm wavelength at t = 4.6 ns is shown in Figure 3(a). Figure 3(b) contains the growth factor (GF = $\eta(t)/\eta_o$) observed for this perturbation as a function of time (solid circles) compared to a LASNEX simulation (solid curve). The simulation is in reasonable agreement with the data, particularly at early times, although it underpredicts the highest growth factor observed.

In order to best demonstrate the differences between perturbation evolution at the embedded interface to that at an ablation front, a normalized growth factor was constructed. The GF for each wavelength at t = 3.2 ns, a time before the onset of significant nonlinearity, was normalized to the GF for λ = 50 μm at this time in both the data and the LASNEX simulations. The

same quantity was constructed for a series of GF simulations and measurements made for perturbations placed at the ablation front of a solid CH(Br) target which was accelerated in a similar fashion to the two-layer target.[9,20,21] These normalized GF are displayed in Figure 4. This comparison between ablation front and embedded interface growth dramatically illustrates the influence of ablative stabilization. While ablation strongly stabilizes short wavelengths, these wavelengths exhibit the highest growth factors observed at the embedded interface. This distinction makes the CH(Br)-Ti embedded interface target an ideal testbed for studying instability evolution in the nonlinear regime, particularly the processes of nonlinear mode coupling and bubble competition.

IV. TWO MODE EXPERIMENTS

A. Mode coupling in Fourier space

After completion of the single-mode experiments described, we began to examine the behavior of an initial spectrum of two or more modes. A modal model for the evolution of such a perturbation where mode coupling is the dominant source of long wavelength structures in the flow is described by Ofer *et al.* [13] Initially, two readily-resolvable initial modes (λ = 10 μm, η_o = 1 μm and λ = 15 μm, η_o = 1 μm) were superimposed in phase. As the growth of the two initial modes proceeds into the nonlinear regime they begin to couple, producing "beat" modes $k_i \pm k_j$, the amplitude of which can be written at second order as

$$\eta_{k_i \pm k_j} \sim (1/2)(k_i \pm k_j)\, \eta_{k_i}^{L}\, \eta_{k_j}^{L} \qquad (1)$$

where $\eta_{k_i}^{L}$ is the spatial amplitude of the mode k_i had the growth been entirely in the linear regime.[11] Here the $k_{\lambda = 10\,\mu m} - k_{\lambda = 15\,\mu m} = k_{\lambda = 30\,\mu m}$ (λ = 30 μm) beat mode should be observed growing up in time.

Figure 5 contains a series of averaged lineouts from the data (left axis) as well as the original pattern (right axis, solid line) imposed at the embedded interface. The curves correspond to lineouts at t = 3.8 ns (dotted curve), 4.3 ns (dashed curve), 4.9 ns (long dashed curve), and 5.3 ns (dot-dashed curve). The imposed pattern is seen growing as time progresses, but the two latest times show a striking qualitative difference from the early time lineouts. The short scale (10 and 15 μm) structures are beginning to give way to a longer scale (30 μm) envelope. By 5.3 ns this effect is quite marked and Fourier analysis should show the amplitude of this longer wavelength mode increasing in time.

A comparison of the Fourier amplitudes of the three modes observed in ℓn(exposure) and the CALE simulations convolved with the instrument MTF is shown in Figure 6. The data and simulations show reasonable agreement and, indeed, a mode at λ = 30 μm, generated from the mode coupling between the 10 and 15 μm modes in the initial spectrum, is observed growing up strongly in the data.

This experiment is an illustration of the process which drives a multimode spectrum toward an inverse cascade late in the nonlinear

development of the instability. A long wavelength feature has been generated via mode coupling between the initial modes, not from the growth of an initially imposed mode. This Fourier-space observation is compelling evidence of the importance of mode coupling processes at a classical, or embedded, interface where stabilization mechanisms for short wavelengths are not present. This process has also been described in terms of a bubble competition process, wherein large structures will, over time, begin to wash smaller-scale structures in the flow downstream. This dominance of large structures will appear as a preponderance of low mode numbers in the Fourier spectrum, which after several generations of mode coupling results in an inverse cascade.

B. Bubble competition in physical space

In the work of Alon *et al.*,[22] the competition between neighboring bubbles is described in a physically-intuitive manner. They begin with an initial velocity field composed of a sum of two modes with wave numbers k and 2k and amplitudes u_1 and u_2, which corresponds to two bubbles with velocities $u_1 \pm u_2$. At early times, the bubbles are seen to rise independently. However, as time progresses the large bubble begins to expand and rise faster, washing its smaller neighbor downstream in the flow. We designed our second two mode experiment to directly investigate the evolution of neighboring bubbles of different sizes as described by Alon. Our target consisted of a superposition of two modes with wave numbers k and 2k

corresponding to wavelengths $\lambda = 20$ μm, $\eta_o = 1$ μm and $\lambda = 10$ μm, $\eta_o = 1$ μm. This same mode structure was utilized by Sadot *et al.* for a Richtmyer-Meshkov bubble-competition experiment done on a shock tube.[23] The pattern produced by this superposition is an alternating series of larger and smaller bubbles side-by-side, and the size and shape of each of the bubbles can be directly observed via face-on radiography. In order to study the corresponding single mode behavior for each of the constituent modes, each of these targets also had, in separate bands, $\lambda = 20$ μm, $\eta_o = 1$ μm and $\lambda = 10$ μm, $\eta_o = 1$ μm.

Figure 7 contains a series of averaged lineouts from the experimental data (left axis) along with the original pattern (solid line, right axis) imposed on the target. The data is uncorrected for instrument response and the lineouts were taken at t = 2.75 ns (dotted curve), 3.25 ns (dashed curve), 3.75 ns (long dashed curve), and 4.25 ns (dot-dashed curve). Qualitatively, this time progression shows the progression of the flow as the larger bubble grows and begins to spread laterally, pushing the smaller neighboring bubble downstream. By t = 4.25 ns, the smaller bubble has all but disappeared from the lineout.

The amplitudes, in ℓn(exposure), of the individual single mode patterns and the constituent modes for the two mode pattern are displayed in Figure 8(a),(b), and (c) respectively along with CALE simulations which have been convolved with the instrument MTF. Both the data and simulations show the amplitude of the 20 μm mode continuing to rise after

the 10 μm mode amplitude has ceased increasing and begins to decrease. This quantitatively describes the behavior noted in the lineouts from the data. The longer wavelength mode at 20 μm is beginning to dominate the 10 μm mode, causing larger-scale structures to begin to dominate the flow and to slow down the progress of the small structures. Figure 9 shows a 2-dimensional CALE simulation at t = 3.75 ns, where the influence of the instrument MTF is not a factor, showing the large bubble beginning to spread and overtake its smaller neighbor.

A comparison of the single mode data in Fig. 8(a) and (b) and the two-mode data in Fig. 8(c) shows the influence of mode coupling on the perturbation evolution. The single mode 10 μm wavelength reaches an amplitude nearly twice that of the 10 μm mode in the two-mode pattern and continues to increase for nearly a nanosecond after the other data shows this mode amplitude beginning to decrease. By examining the evolution of the three patterns on a single target we are able to remove the influence of variations in the drive or target conditions and can attribute such differences to the influence of mode coupling. The greatest limitation to the experiment is that the bubbles are growing up into a finite thickness layer of titanium. This limits their amplitude in areal density, $\delta(\rho r)$, since there is a finite amount of Ti present to flow into the spikes, and also in absolute spatial magnitude since the rising bubbles will eventually break through the rear surface of the titanium payload. This limitation on the timescale over which the flow may evolve does not allow us to follow the bubble competition

process to the latest stages of development. A bubble competition analysis may also be possible.[24] **{Bruce: References to unpublished or to be submitted work are not permitted.}**

V. MULTIMODE EXPERIMENTS

In an attempt to develop an experimental test for recent modal models,[10,13] we next imposed a multimode pattern at the embedded interface consisting of a "continuous" spectrum (harmonics 1-19, fundamental λ = 200 μm). The continuous spectrum examines the emergence of long wavelength features in the flow from both seeding via mode coupling and growth from wavelengths present in the initial spectrum.

Figure 10 shows the results from one such experiment utilizing the 20 mode continuous spectrum target with a fundamental wavelength of λ = 200 μm. Figure 10(a) shows the initial pattern (right axis, dashed curve) imposed at the embedded interface and a lineout from the data in ln(exposure) at t = 4.6 ns (left axis, solid curve). The features of the original pattern are seen in the data, with no clear change in the shape of the rippled pattern or transition to larger scale features. The Fourier spectrum shown in Figure 10(b) confirms this conclusion. Growth of the initial mode spectrum is observed but the lowest mode numbers have not begun to dominate the growth. The mode amplitudes in ℓn(exposure) are shown both uncorrected and then corrected for MTF. To produce the "corrected" spectrum, each mode amplitude was simply divided by the value of the MTF at that wavelength. It appears that

the duration of the acceleration is not long enough to allow evolution well into the nonlinear regime and the several generations of coupling necessary to see a true inverse cascade. Additionally, the Ti layer thickness is much less than the perturbation wavelengths, which may impede the growth as discussed at the end of Sec. IV,B. [Will insert CALE simulations if Steve has any done by end of next week.]

VI. CONCLUSION AND SUMMARY

We have performed a series of experiments investigating the evolution of both single- and multimode initial perturbations at a Rayleigh-Taylor-unstable embedded interface. The data are compared with simulations done with either the LASNEX or CALE codes. Data from the single mode experiments show good agreement with the simulations and, when compared to ablation front results in terms of a normalized growth factor, illustrate the strong growth of short wavelengths ($\lambda \sim$ 10-20 μm) in the absence of ablation.

The experiments were then extended to the study of a superposition of two modes. The first experiment described placed a superposition of $\lambda = 10$ and 15 μm at the embedded interface. As the growth of these two modes proceeds into the nonlinear regime, they begin to couple and generate a beat mode at $\lambda = 30$ μm. The development of these three modes in time as observed in the data is in reasonable agreement with CALE simulations. This experiment clearly demonstrates the production of new modes in the

spectrum via mode coupling. This experiment is best understood in terms of the modal model described by Ofer *et al.* [13] wherein the saturation model of Haan [10,12] is extended to the case where mode generation via coupling is a significant effect.

In an attempt to develop an experiment which directly probes the process of bubble competition, we performed a series of experiments utilizing a target based upon one studied numerically by Alon *et al.* [22] Here two modes with wave numbers k and 2k (λ = 10 and 20 μm) are superposed resulting in a pattern which appears in physical space as a large bubble sitting next to a smaller neighbor. Lineouts from the data show that as time progresses, the smaller bubble is washed downstream by its larger neighbor. By comparing the amplitudes of the two modes present in this pattern to the evolution of their single mode counterparts under identical conditions (they were present in separate bands on the same target) clearly shows the influence of mode coupling processes on the evolution of the individual modes. The single mode λ = 10 μm pattern exhibits an increasing amplitude for ~ 1 ns after the short wavelength (λ = 10 μm) mode in the two-mode pattern has begun to decrease.

Finally a multimode initial spectrum consisting of either a discrete band or quasi-continuous sequence of modes was imposed at the embedded interface to attempt to experimentally observe the predicted inverse cascade toward low mode numbers (long wavelengths). Data for a 20-mode quasi-continuous spectrum was presented which showed growth of the initial

modes but not significant tendency toward long wavelength structures dominating the flow. A longer period of acceleration appears to be required to generate the several generations of coupling required to observe a true cascade.

VII. ACKNOWLEDGEMENTS

The authors would like to thank H. Louis, T. Demiris and R. Wallace for the outstanding target fabrication and characterization performed for these experiments and the expert technical staff at Nova for their support. The authors further express their gratitude to S. Haan, D. Shvarts, U. Alon, and D. Ofer for many fruitful discussions and suggestions regarding this work. This work was performed by the Lawrence Livermore National Laboratory under the auspices of the U. S. Department of Energy under Contract No. W-7405-ENG-48.

X. REFERENCES

[1]Lord Rayleigh, Proc. London Math Soc. **14**, 170 (1883).

[2]G. Taylor, Proc. R. Soc. London Ser. A **301**, 192 (1950).

[3]J. D. Lindl and W. C. Mead, Phys. Rev. Lett. **34**, 1273 (1975).

[4]C. P. Verdon, R. L. McCrory, R. L. Morse, G. R. Baker, D. I. Meiron, and S. A. Orszag, Phys. Fluids **25**, 1653 (1982).

[5]S. E. Bodner, Phys. Rev. Lett. **33**, 761 (1974).

[6]J. Lindl, Phys. Plasmas **2**, 3933 (1995).

[7]E. Muller, B. Fryxell, and D. Arnett, Astron. Astrophys. **251**, 505 (1991).

[8]M. Herant and S. E. Woosley, Ap. J. **425**, 814 (1994).

[9]K. S. Budil, B. A. Remington, T. A. Peyser, K. O. Mikaelian, P. L. Miller, N. C. Woolsey, W. M. Wood-Vasey, and A. M. Rubenchik, Phys. Rev. Lett. **76** (24), 4536-4539 (1996).

[10]S. W. Haan, Phys. Rev. A **39**, 5812 (1989).

[11]D. L. Young, Physica D **12**, 32 (1984).

[12]S. W. Haan, Phys. Fluids B **3**, 2349 (1991).

[13]D. Ofer, U. Alon, D. Shvarts, R. L. McCrory, and C. P. Verdon, Phys. Plasmas **3** (8), 3073-3090 (1996).

[14]D. Layzer, Ap. J. **122**, 1 (1955).

[15]S. N. Dixit, Appl. Opt. **32**, 2543 (1993).

[16]S. N. Dixit, M. D. Feit, M. D. Perry, and H. T. Powell, Opt. Lett. **21**, 1715 (1996).

[17]K. S. Budil, T. S. Perry, P. M. Bell, J. D. Hares, P. L. Miller, T. A. Peyser, R. Wallace, H. Louis, and D. E. Smith, Rev. Sci. Instrum. **67**, 485 (1996).

[18]G. B. Zimmerman and W. L. Kruer, Comments Plasma Phys. Controlled Fusion **2**, 51 (1975).

[19]H. Louis, A. Demiris, K. S. Budil, P. L. Miller, T. A. Peyser, P. E. Stry, D. A. Wojtowicz, and P. E. Dimotakis, J. Fusion Tech. **28**, 1769 (1995).

[20]B. A. Remington, S. W. Haan, S. G. Glendinning, J. D. Kilkenny, D. H. Munro, and R. J. Wallace, Phys. Fluids B **4** (4), 967-978 (1992).

[21]B. A. Remington, S. V. Weber, M. M. Marinak, S. W. Haan, J. D. Kilkenny, S. G. Glendinning, and R. J. Wallace, Phys. Plasmas **2**, 241 (1995).

[22]U. Alon, J. Hecht, D. Ofer, and D. Shvarts, Phys. Rev. Lett. **74** (4), 534-537 (1995).

[23]O. Sadot, L. Erez, G. Erez, G. Ben-Dor, L. A. Levin, D. Shvarts, U. Alon, and D. Oron, presented at the 6th International Workshop on the Physics of Compressible Turbulent Mixing, Marseille, France, June 18-21, 1997 (unpublished).

[24]D. Shvarts, in preparation (1997).

IX. FIGURE CAPTIONS

Figure 1: Experimental configuration for the classical Rayleigh-Taylor instability studies.

Figure 2: (a) Laser power profile (left axis) and measured time history of the radiation temperature (right axis) in the hohlraum. (b) Measured trajectory (left axis) of the rear surface of the CH(Br)-Ti composite target and corresponding LASNEX calculation of the foil motion and the acceleration profile felt by the CH(Br)-Ti interface as predicted by LASNEX (right axis). Please note the offset scales on the left and right axes.

Figure 3: (a) Example radiograph of the CH(Br)-Ti composite target with a single mode $\lambda = 20$ μm, $\eta_o = 1.0$ μm perturbation at t = 4.6 ns. (b) Amplitude in ℓn(exposure) as a function of time for single mode $\lambda = 20$ μm, $\eta_o = 1.0$ μm, uncorrected for instrument response. The solid line represents the results of a LASNEX simulation after it has been convolved with the instrument modulation transfer function.

Figure 4: Normalized growth factor (GF(λ)/GF(λ=50 μm)) at t = 3.2 ns for both the embedded interface (ei) and the ablation front (af). The solid and dot-dashed curves were constructed from LASNEX simulations of these experiments.

Figure 5: The thick solid line is the imposed perturbation for the two-mode $\lambda = 10$ μm, $\eta_o = 1.0$ μm + $\lambda = 15$ μm, $\eta_o = 1.0$ μm pattern (right axis). The other curves represent lineouts from the data at t = 3.8 ns (dotted curve), 4.3 ns (dashed curve), 4.9 ns (long dashed curve), and 5.3 ns (dot-dashed curve).

Figure 6: Amplitude in ℓn(exposure) as a function of time for the $\lambda = 10$, 15 and 30 μm modes, uncorrected for instrument response. The curves represent CALE simulations which have been convolved with the instrument modulation transfer function.

Figure 7: The thick solid line is the imposed perturbation for the two-mode λ = 10 μm, η_o = 1.0 μm + λ = 20 μm, η_o = 1.0 μm pattern (right axis). The other curves represent lineouts from the data at t = 2.75 ns (dotted curve), 3.25 ns (dashed curve), 3.75 ns (long dashed curve), and 4.25 ns (dot-dashed curve).

Figure 8: Amplitude in ℓn(exposure) as a function of time for the λ = 10 and 20 μm modes in the 2-mode bubble merger target, uncorrected for instrument response. The curves represent CALE simulations which have been convolved with the instrument modulation transfer function.

Figure 9: Two-dimensional density plot from a CALE simulation of the bubble merger target at t = 3.75 ns.

Figure 10: (a) Imposed 20-mode pattern as designed (right axis, dashed curve) and as observed in the data at t = 4.6 ns (left axis, solid curve). (b) Amplitude in ℓn(exposure) at t = 4.6 ns for the 20-mode pattern, shown both uncorrected (checkered) and corrected for instrument response (solid bars).

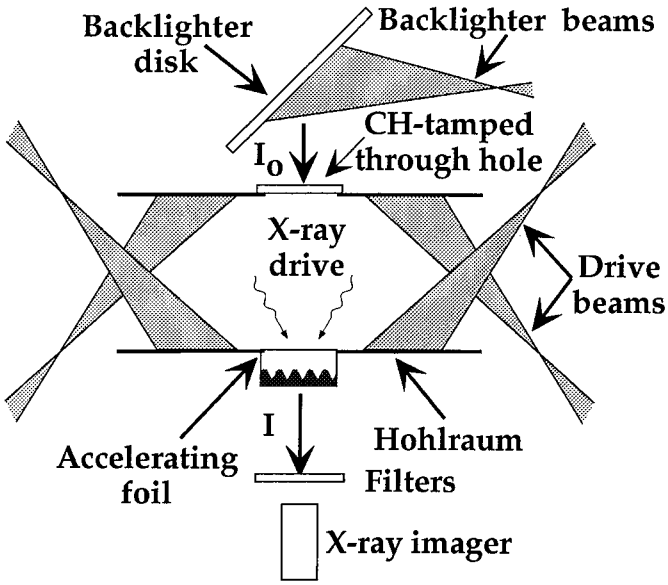
Backlighter disk
Backlighter beams
CH-tamped through hole
I_o
X-ray drive
Drive beams
I
Accelerating foil
Hohlraum
Filters
X-ray imager

Figure 1

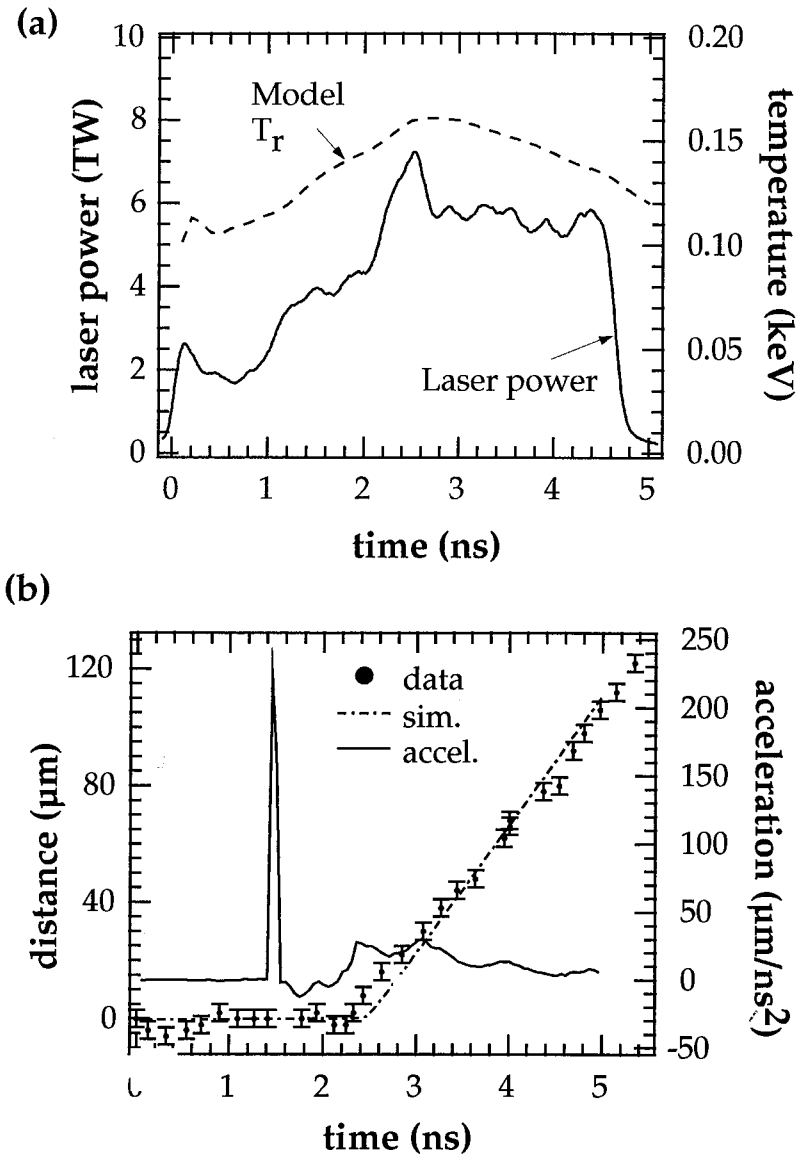
(a)
Model
T_r
Laser power
laser power (TW)
temperature (keV)
time (ns)
(b)
data
sim.
accel.
distance (μm)
acceleration (μm/ns²)
time (ns)

Figure 2

(a)

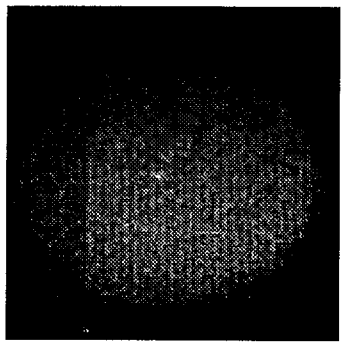

(b)

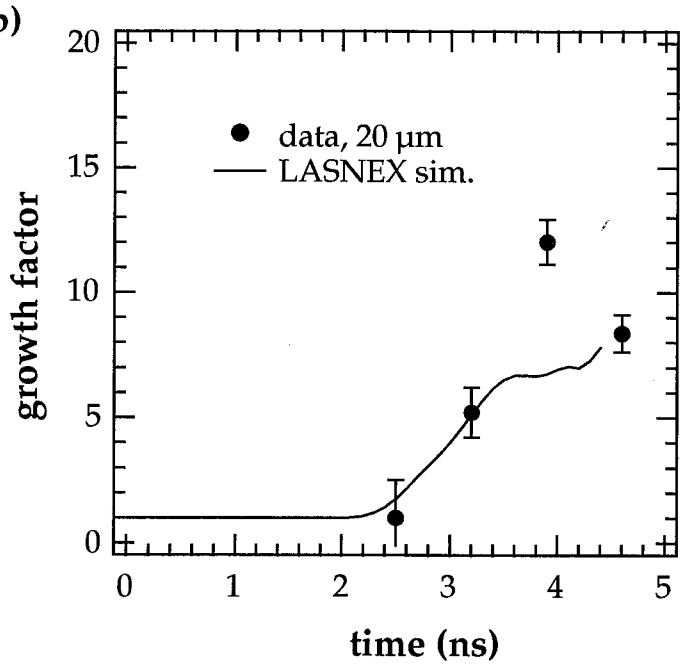

Figure 3

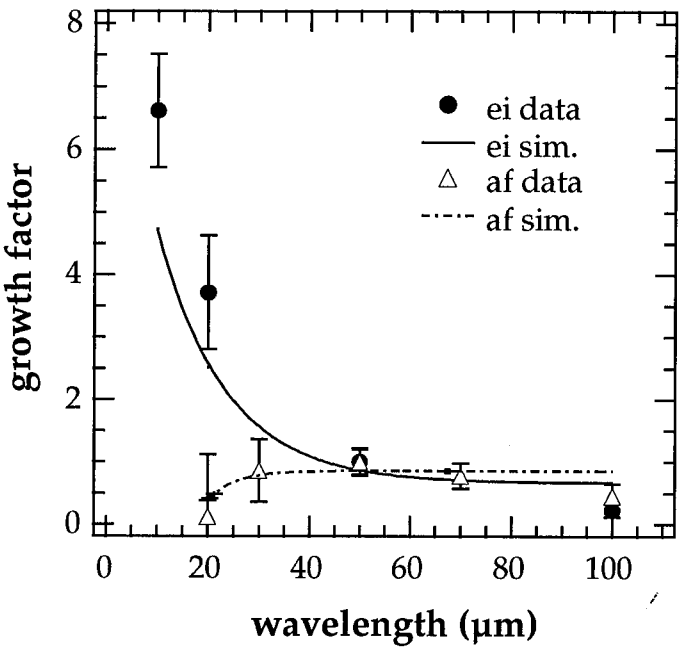
growth factor
wavelength (μm)
ei data
ei sim.
af data
af sim.
0
2
4
6
8
0
20
40
60
80
100

Figure 4

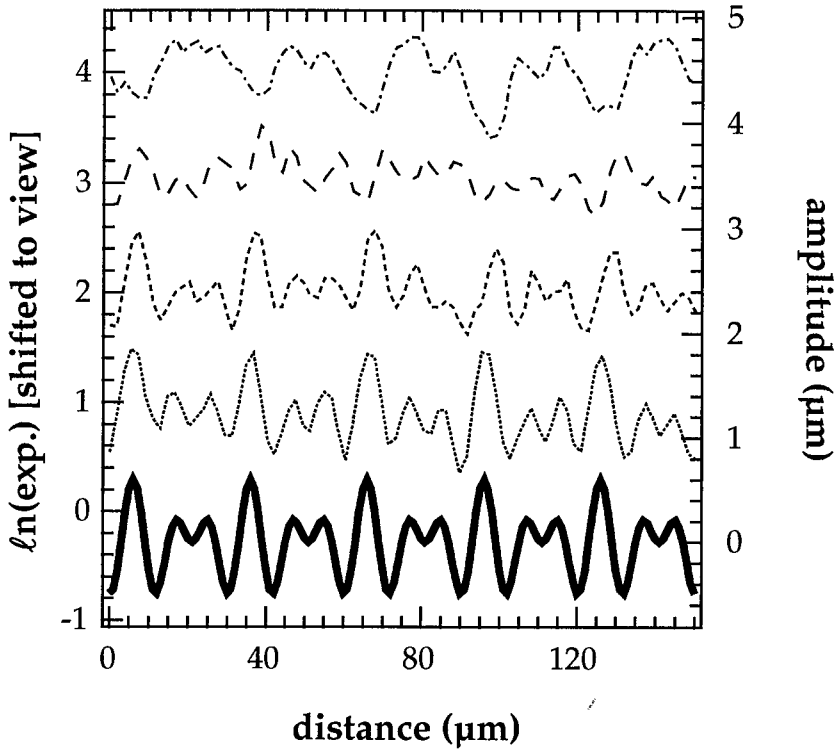
ℓn(exp.) [shifted to view]
amplitude (μm)
distance (μm)
-1
0
1
2
3
4
5
0
40
80
120

Figure 5

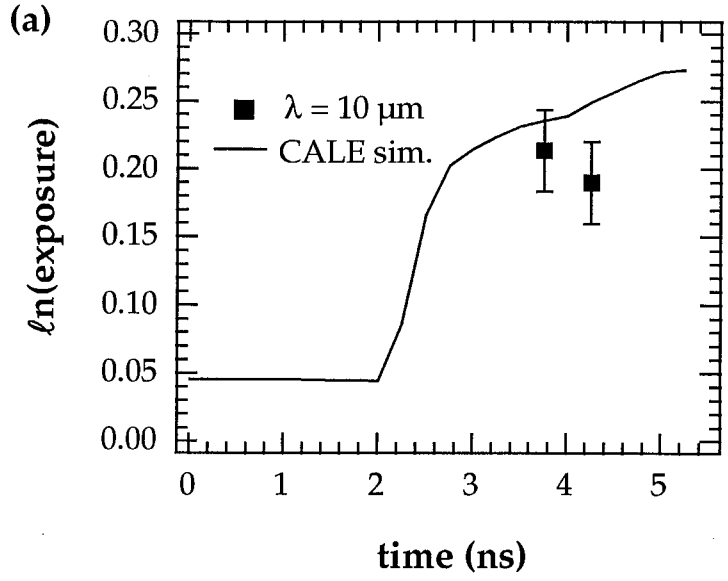
(a)
0.30
0.25
0.20
0.15
0.10
0.05
0.00
ℓn(exposure)
λ = 10 μm
CALE sim.
0
1
2
3
4
5
time (ns)

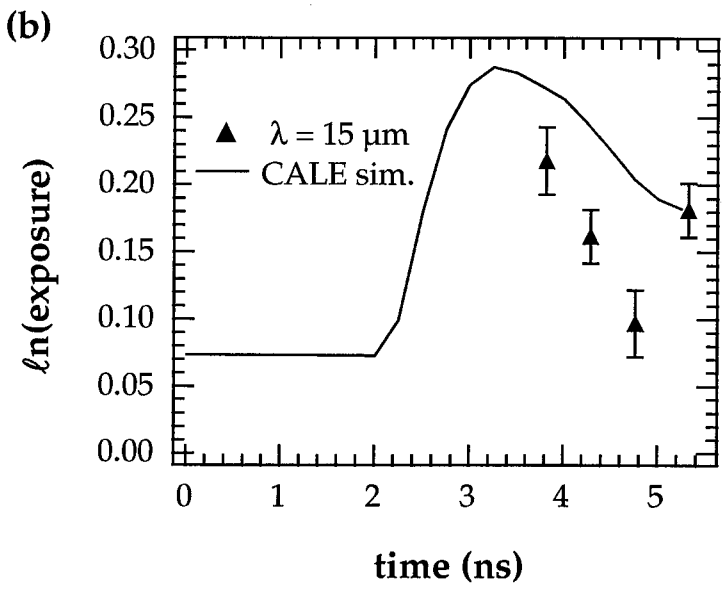
(b)
0.30
0.25
0.20
0.15
0.10
0.05
0.00
ℓn(exposure)
λ = 15 μm
CALE sim.
0
1
2
3
4
5
time (ns)

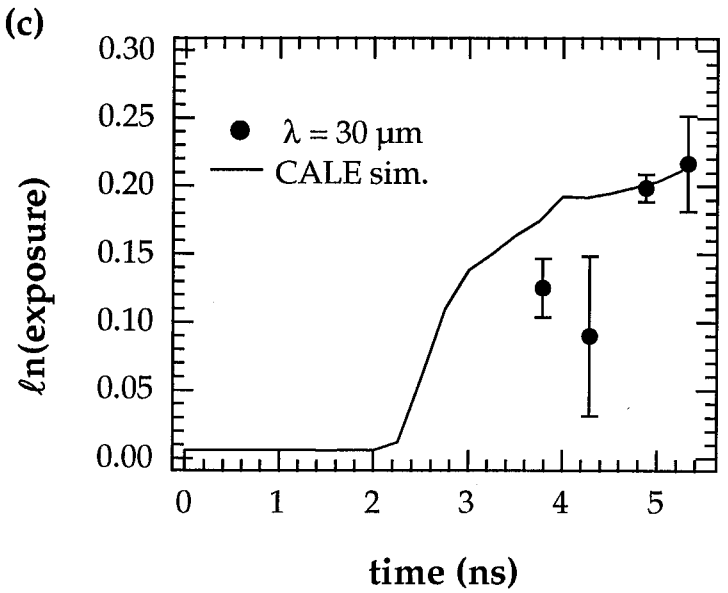
(c)
0.30
0.25
0.20
0.15
0.10
0.05
0.00
ℓn(exposure)
λ = 30 μm
CALE sim.
0
1
2
3
4
5
time (ns)

Figure 6

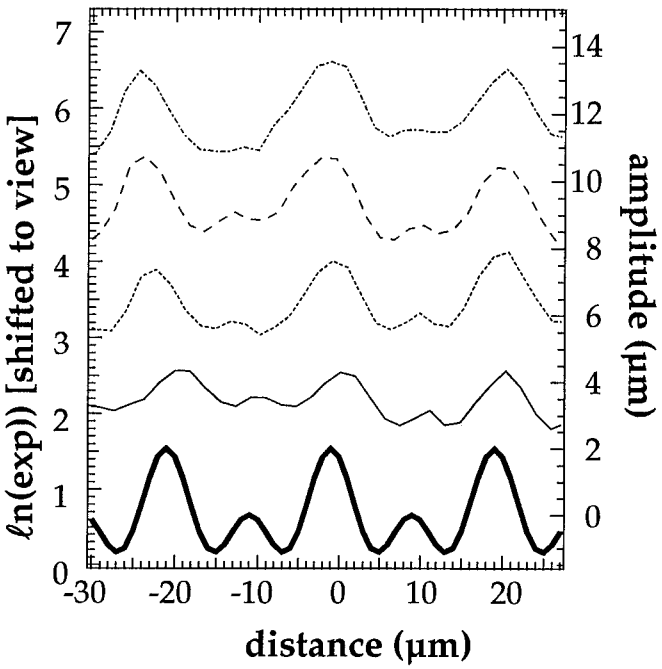
ℓn(exp)) [shifted to view]
amplitude (μm)
distance (μm)
0
1
2
3
4
5
6
7
0
2
4
6
8
10
12
14
-30
-20
-10
0
10
20

Figure 7

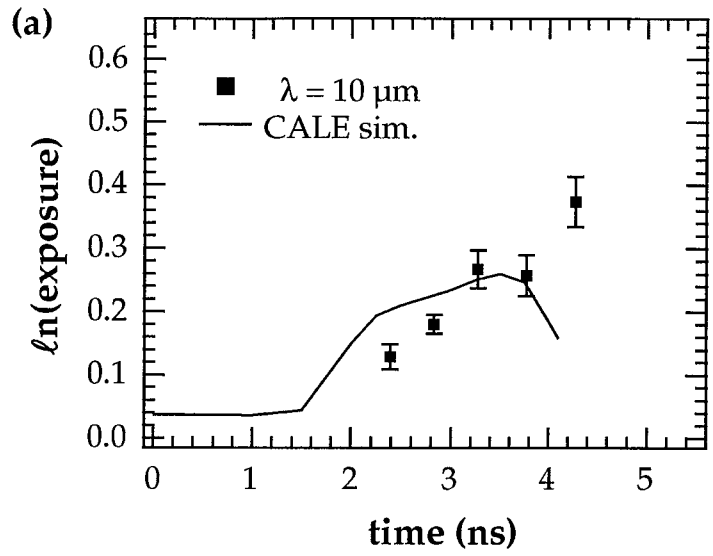
(a)
λ = 10 μm
CALE sim.
ℓn(exposure)
time (ns)

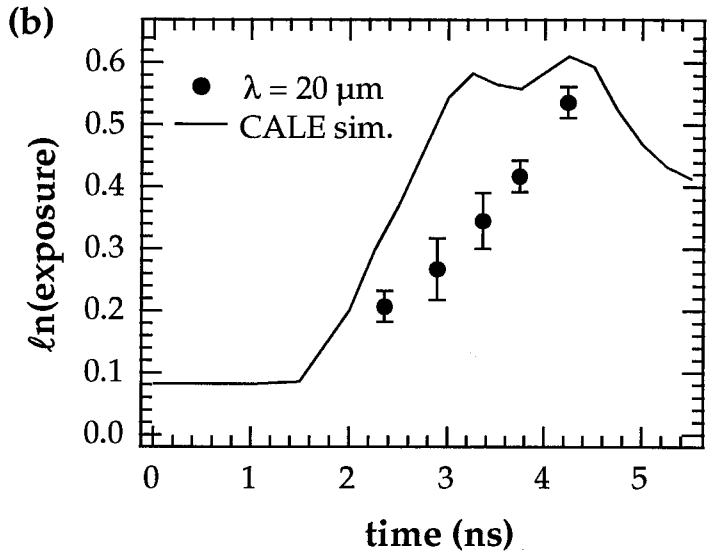
(b)
λ = 20 μm
CALE sim.
ℓn(exposure)
time (ns)

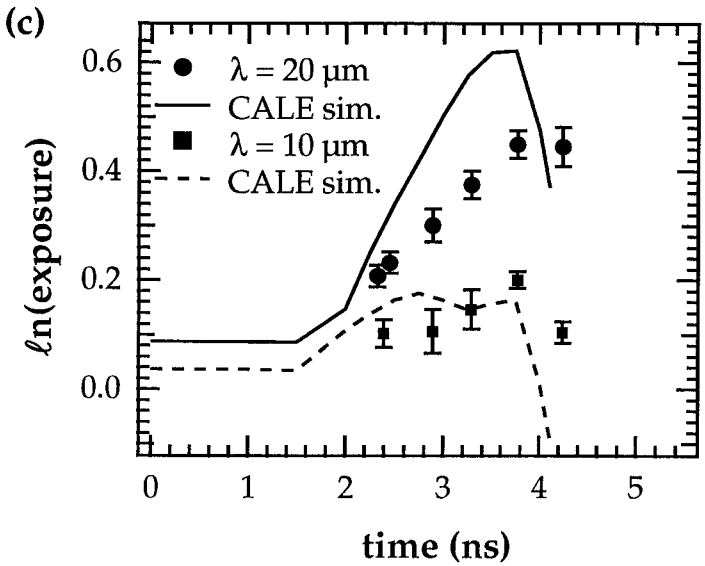
(c)
λ = 20 μm
CALE sim.
λ = 10 μm
CALE sim.
ℓn(exposure)
time (ns)

Figure 8

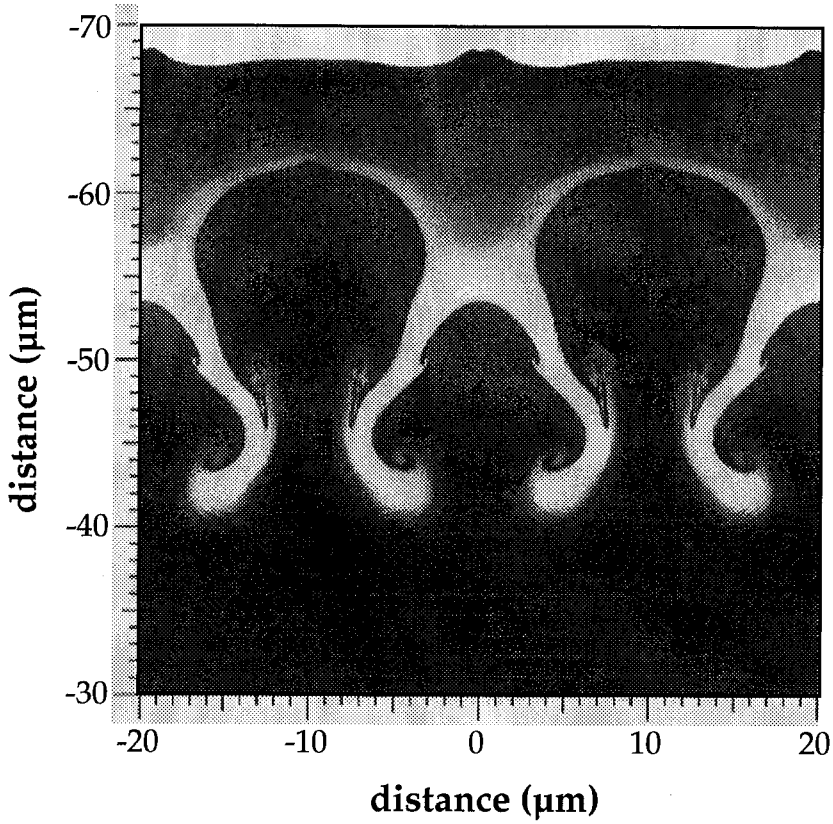

Figure 9

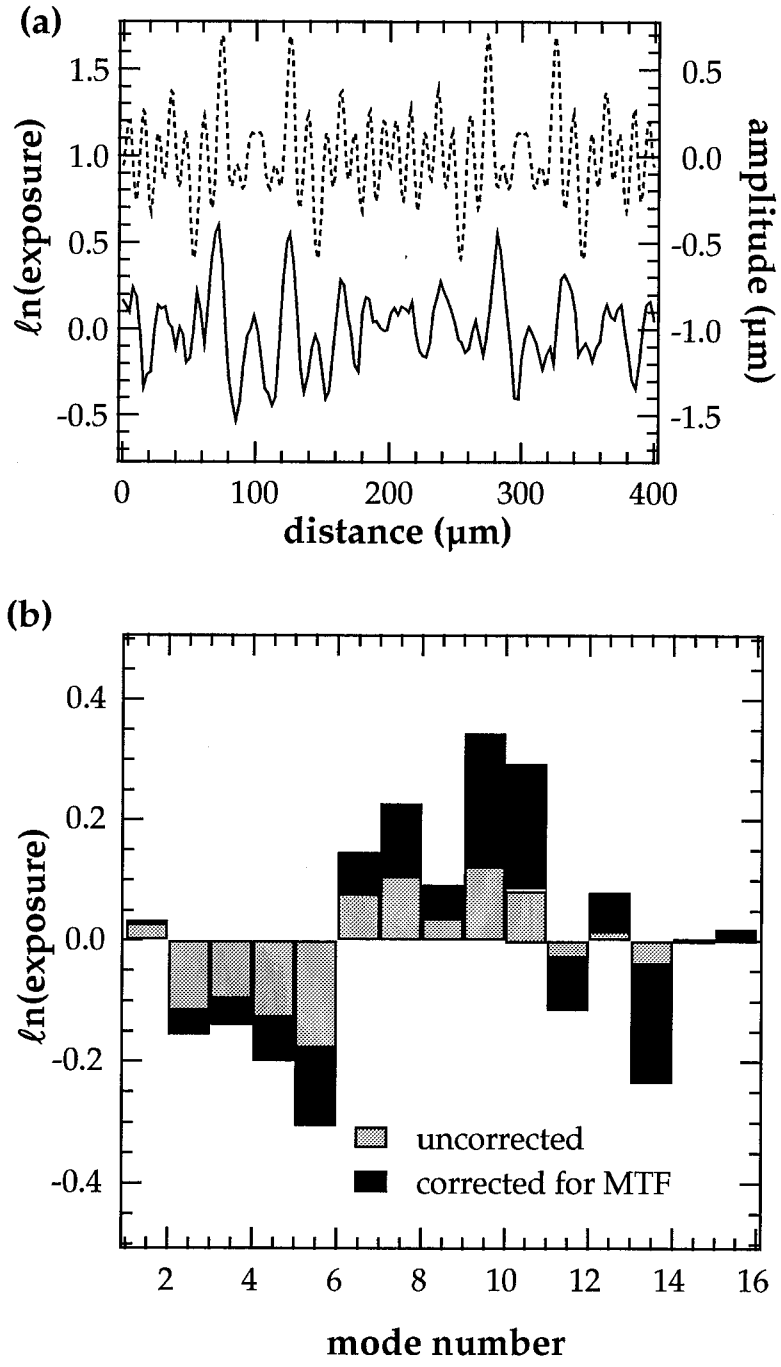
(a)
1.5
1.0
0.5
0.0
-0.5
ℓn(exposure)
0.5
0.0
-0.5
-1.0
-1.5
amplitude (μm)
0
100
200
300
400
distance (μm)
(b)
0.4
0.2
0.0
-0.2
-0.4
ℓn(exposure)
uncorrected
corrected for MTF
2
4
6
8
10
12
14
16
mode number

Figure 10

Technical Information Department • Lawrence Livermore National Laboratory
University of California • Livermore, California 94551